AD-A114 365 AEROSPACE CORP EL SEGUNDO CA SPACE SCIENCES LAB F/G 4/1
AURORAL PARTICLE DISTRIBUTION FUNCTIONS AND THEIR RELATIONSHIPS--ETC(U)
APR 82 J F FENNELL, D J GORNEY, P F MIZERA F04701-81-C-0082
UNCLASSIFIED TR-0082(2940-05)-6 SD-TR-82-23 NL

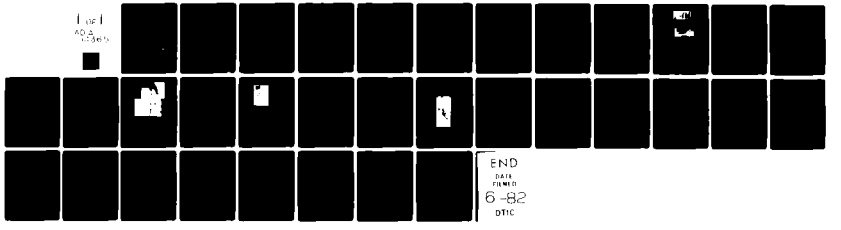

REPORT SD-TR-82-23

Auroral Particle Distribution Functions and Their Relationships to Inverted Vs and Auroral Arcs

J. F. FENNELL, D. J. GORNEY,
and P. F. MIZERA
Space Sciences Laboratory
Laboratory Operations
The Aerospace Corporation
El Segundo, Calif. 90245

12 April 1982

Prepared for
SPACE DIVISION
AIR FORCE SYSTEMS COMMAND
Los Angeles Air Force Station
P.O. Box 92960, Worldway Postal Center
Los Angeles, Calif. 90009

This report was submitted by The Aerospace Corporation, El Segundo, CA 90245, under Contract No. F04701-81-C-0082 with the Space Division, Deputy for Technology, P.O. Box 92960, Worldway Postal Center, Los Angeles, CA 90009. It was reviewed and approved for The Aerospace Corporation by H. R. Rugge, Director, Space Sciences Laboratory. Major G. A. Kuck, SD/YLS, was the project officer for the Mission-Oriented Investigation and Experimentation (MOIE) Program.

This report has been reviewed by the Public Affairs Office (PAS) and is releasable to the National Technical Information Service (NTIS). At NTIS, it will be available to the general public, including foreign nations.

This technical report has been reviewed and is approved for publication. Publication of this report does not constitute Air Force approval of the report's findings or conclusions. It is published only for the exchange and stimulation of ideas.

George A. Kuck, Major, USAF
Project Officer

Florian P. Meinhart, Lt Col, USAF
Director of Advanced Space Development

FOR THE COMMANDER

Norman L. Lee, Jr., Colonel, USAF
Deputy for Technology

UNCLASSIFIED

SECURITY CLASSIFICATION OF THIS PAGE *(When Data Entered)*

REPORT DOCUMENTATION PAGE		READ INSTRUCTIONS BEFORE COMPLETING FORM
1. REPORT NUMBER SD-TR-82-23	2. GOVT ACCESSION NO. AD-A114 365	3. RECIPIENT'S CATALOG NUMBER
4. TITLE *(and Subtitle)* AURORAL PARTICLE DISTRIBUTION FUNCTIONS AND THEIR RELATIONSHIP TO INVERTED Vs AND AURORAL ARCS		5. TYPE OF REPORT & PERIOD COVERED 6. PERFORMING ORG. REPORT NUMBER TR-0082(2940-05)-6
7. AUTHOR(s) J. F. Fennell, D. J. Gorney, and P. F. Mizera		8. CONTRACT OR GRANT NUMBER(s) F04701-81-C-0082
9. PERFORMING ORGANIZATION NAME AND ADDRESS The Aerospace Corporation El Segundo, California 90245		10. PROGRAM ELEMENT, PROJECT, TASK AREA & WORK UNIT NUMBERS
11. CONTROLLING OFFICE NAME AND ADDRESS Space Division Air Force Systems Command Los Angeles, California 90009		12. REPORT DATE 12 April 1982 13. NUMBER OF PAGES 31
14. MONITORING AGENCY NAME & ADDRESS*(if different from Controlling Office)*		15. SECURITY CLASS. *(of this report)* Unclassified 15a. DECLASSIFICATION/DOWNGRADING SCHEDULE

16. DISTRIBUTION STATEMENT *(of this Report)*

Approved for public release; distribution unlimited.

17. DISTRIBUTION STATEMENT *(of the abstract entered in Block 20, if different from Report)*

18. SUPPLEMENTARY NOTES

19. KEY WORDS *(Continue on reverse side if necessary and identify by block number)*

Aurora
Particle Distributions
Polar Plasmas

20. ABSTRACT *(Continue on reverse side if necessary and identify by block number)*

Utilizing data from three satellites we show the relationship between the particle energy and angular distributions, the resulting auroral forms, and spatial features such as the inverted V and electrostatic structures. The occurrence of field-aligned electrons over a wide range of energies near and at the edges of inverted V structures in the low altitude local evening auroral region is an outstanding feature in the data. The DMSP pictures often show a brightening of the auroral form in coincidence with similar intense electron precipitation at the edges of inverted V structures. Preliminary examination

DD FORM 1473 (FACSIMILE)

UNCLASSIFIED

SECURITY CLASSIFICATION OF THIS PAGE *(When Data Entered)*

19. KEY WORDS (Continued)

20. ABSTRACT (Continued)

of the S3-3 data has produced only a few such events with a tendency for them to occur at lower altitudes. As a separate topic, a detailed description of a high altitude inverted V structure is presented using S3-3 data. The region contained strong perpendicular electric field structures embedded therein. The potential drop in the region peaks near 16 kV with 10-12 kV below and 4-6 kV above 8000 km. The modification of the electron distributions due to strong electric field structures is analyzed. The signature of the acceleration in the electrons is consistent with an acceleration region that starts 2000-4000 km above the satellite altitude of 8000 km and extends well below the satellite.

Acknowledgments

We would like to thank all those people who made this study possible. Special thanks goes to V. Bledsoe, D. Croley and A. Clarke for organizing the data sets and providing computational support. Thanks also goes to D. Croley, Y. Chiu and M. Schulz for many useful discussions concerning these data. The data reduction and analysis was supported partly by the U. S. Air Force under Contract No. F04701-79-C-0080 and partly by the National Science Foundation under Contract No. ATM-8000518.

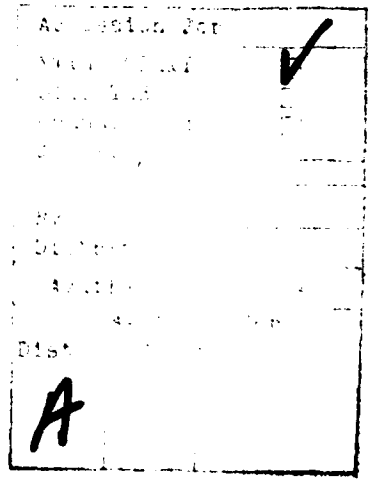

CONTENTS

FIGURES

Introduction

There have been available for some time now several comprehensive satellite data sets which contain detailed measurements of the auroral particle spectra (Frank and Ackerson, 1972; Hoffman and Burch, 1973; Winningham et al., 1975; Burch et al., 1975; Meng et al., 1976; Mizera et al., 1976; Mizera and Fennell, 1977; Ghielmetti et al., 1978; and others), and in a few cases auroral imaging (Rogers et al., 1974; Anger and Lui, 1973). The so-called inverted V structure has been associated with auroral arcs (Ackerson and Frank, 1972a, b; Frank and Ackerson, 1972; Mizera et al., 1975; Meng, 1976). The particle observations were usually made at low to medium altitudes on satellites and rockets which measured precipitating particles, and the results were compared with photographs of auroral structures. The field aligned nature of the precipitating electrons in the auroral regions was observed by many experimenters. Comparisons of low altitude particle distributions with auroral forms has led to a recognition that the correlation of the inverted V structure and bright forms is more than a crude spatial relationship. There are features in the visual forms which have direct counterparts to features of the particle precipitation. One such feature often occurs near the edges of the inverted V structure and is discussed below.

A second and equally interesting development has been the recent ability to examine the auroral particle distributions within the acceleration region itself (Mizera and Fennell, 1977; Mizera et al., 1980; Mozer et al., 1977; Sharp et al., 1979; Torbert and Mozer, 1978). Of particular interest in this report is the effect that the "electrostatic shocks" (Mozer et al., 1977; Torbert and Mozer, 1978) have on the particle distributions. As is discussed below, the particle distributions can be used to infer the extent of the

acceleration region along an auroral field line.

In order to treat these subjects we have brought together data from three different USAF satellites, namely the P72-1, the DMSP, and the S3-3. The strengths of each data set are utilized to enhance our understanding of the phenomena. The primary features of the data sets are: 1) the good angular resolution of the P72-1 data at low altitude (~ 800 km circular polar orbit), 2) the combination of simultaneous precipitating electron spectra, auroral X-rays and photographic auroral images (image only on DMSP-29) from the DMSP satellites (~ 800 km altitude, dawn-dusk polar orbits), and 3) the good angular distributions of electrons and ions plus electric field measurements within the auroral acceleration region from the S3-3 satellite (250 x 8200 km altitude polar orbit). The details of the experiments have been described elsewhere (Rogers et al., 1976; Mizera and Fennell, 1977; Mozer et al., 1977; Eather, 1979; Meng, 1979).

By combining the basic results from these sets of measurements we can arrive at an understanding of the auroral processes which is not possible from an individual data set.

Field Aligned Electrons Over Wide Energy Ranges

We will first examine the low altitude inverted V electron signature. The field aligned nature of the precipitating electrons in the inverted V regions has been described by many experimenters on both rockets and satellites. Generally, the angular distributions of the electrons in the inverted V were found to be field aligned for energies corresponding to the peak of the precipitating electron spectrum (Mizera et al., 1976).

Figure 1 shows an electron spectrogram from the P72-1 satellite (top

(a)

(b)

Fig. 1. (a) Spectrogram of Late Evening Auroral Electrons Taken on February 13, 1974 by the P72-1 Satellite. Intensity is proportional to electron energy flux. An inverted V structure is centered near 39480 sec.

(b) Auroral Photograph Taken by the DMSP Satellite at 1058 UT on February 13, 1974. The Trajectories of the DMSP (dashed line) and P72-1 (solid line) satellites are shown along with the time (left-hand scales). The P72-1 satellite crosses an auroral form near 39480 sec which corresponds to the inverted V structure in Figure 1(a).

panel) and the corresponding auroral photograph from the DMSP satellite (bottom panel) taken on February 13, 1974. Both satellites are near 800 km altitude in the northern premidnight auroral region. As can be seen in the bottom panel of Figure 1 both satellites crossed the auroral form near 39500 sec. This is near the peak of the inverted V in the top panel. The peak energy of the inverted V can be seen to be near 10 keV on the spectrogram.

DMSP is moving equatorward and P72-1 is moving poleward so that the satellites have simultaneous coverage only at 39500 sec. All of our comments assume that the auroral forms shown in the DMSP image were present when P72-1 traversed the region.

As P72-1 proceeded poleward near 39525 sec UT, it encountered a strong precipitation over a range of energies, lasting less than 12 seconds. Careful examination of the auroral photograph shows a very thin auroral "wisp" near the P72-1 ground track (within the errors of the mapping) near 39525-39530 sec. This "wisp" may be an isolated narrow arc. The "wisp" intensity does not appear as great as the main arc, although the particle fluxes estimated from the spectrogram are quite intense.

The details of the inverted V for selected satellite spins from P72-1 are shown in the bottom panels of Figure 2. The satellite spin period is ~ 5 sec. Note that the energy at which the electron distributions peak near 0° pitch angle increases from 0.62 to 1 keV at $\Lambda \sim 69.5°$ to ~ 9.7 keV at $\Lambda \sim 70.8$. The energy then rapidly decreases (not shown in complete detail) again at higher latitude. This is the classic inverted V structure as seen by an experiment which measures both electron energy and pitch angle. Such angular distributions and energy dependent field aligned fluxes have been used to evidence the existence of quasi-static parallel electric fields (Evans,

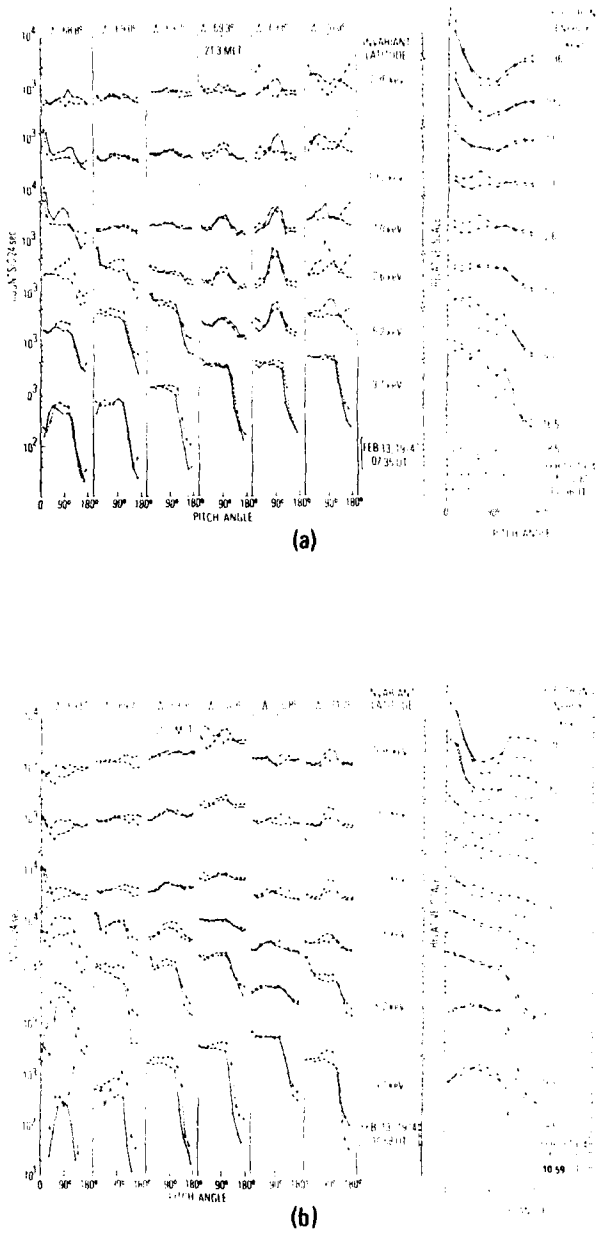

Fig. 2. Electron Pitch Angle Distributions at Various Energies in the Inverted V of Figure 1 (bottom panel) and for an Inverted V Encountered ~ 3.5 Hours Earlier (top panel). The right-most panels correspond to the strong field aligned fluxes over a range of energies which occur just poleward of the inverted Vs.

1974; Mizera et al., 1976).

The intense field-aligned fluxes that were observed just poleward of the inverted V in Figure 1 are shown in the bottom right panel of Figure 2. The low energy electrons are much more strongly field aligned than the higher energy fluxes. The electrons are field aligned from 0.36 to 9.7 keV. In this case the field alignment over the wide energy range existed only during one spin period.

This field alignment at the edge of an inverted V structure is not uncommon. Another example is shown at the top of Figure 2. These data were taken ~ 3.5 hours earlier in the same region. Again, we see the signature of the inverted V structure with the energy of the field aligned electron flux increasing from 0.62-1.0 keV at $\Lambda \sim 68.8°$ to 9.7 keV at $\Lambda \sim 69.3$. The field alignment disappeared and the peak energy decreased at higher altitude. At the poleward edge we once again observed a strong field alignment of electrons over a wide energy range (0.36 to 16.5 keV). The lower energy electrons again showed much stronger field alignments.

As can be seen in Figure 2, the field aligned fluxes are generally well within the atmospheric loss cone (~ 60° for these data) and the backscatter flux is usually much less than the downward fluxes in these edge regions. This is generally not the case at the center of the inverted V, where the fluxes below the energy peak are often observed to be isotropic.

It has been argued that such field alignment of the auroral electrons over a wide range of energies is not consistent with a quasi-static parallel electric field acceleration (Whalen and Daly, 1979). We refer the reader to that paper for a discussion of a possible mechanism.

We showed in Figure 1 that the inverted V edge feature (field aligned

fluxes) appeared to correspond to a discreet auroral form or "wisp". Do all such features correspond to auroral forms? Do these edge features correspond to a low altitude auroral process? In order to shed more light on this subject we must examine evidence from other observations.

Enhancements in the precipitating electron energy flux over a wide range of energies often appear in the DMSP data at low altitude. Since the DMSP satellite instrument measures only precipitating electron fluxes, we cannot tell if these enhanced fluxes are field aligned, but the strong similarities with the P72-1 inverted V profiles is compelling. If we assume the intense precipitating fluxes at the edges of the inverted Vs are the field aligned fluxes, we can then examine the auroral forms to see if there are optical features associated with such fluxes.

We present only one example of the many particle spectrogram and auroral pictures we have examined. Figure 3 shows a composite of auroral forms, bremsstrahlung X-rays and precipitating electron fluxes for December 2, 1977. The inverted V structure near 45430 sec UT is reminiscent of Figure 2a. The electron fluxes show strong precipitation at both edges. Examination of the auroral form shows a brightening of the emission at both positions. (The particle fluxes must be mapped from 800 km altitude along the field line to 100 km altitude. This amounts to shifting the electron fluxes poleward in time by 5 - 6 seconds.) Thus, in this instance the "edge" feature corresponds to "discrete" auroral emissions.

Basically, we found that when the maximum energy and intensity of the edge features were comparable to those of the center of the inverted V itself then auroral forms or brightening of the form were observed at that point in the DMSP data. If the edge feature had high energy-flux but low compared to

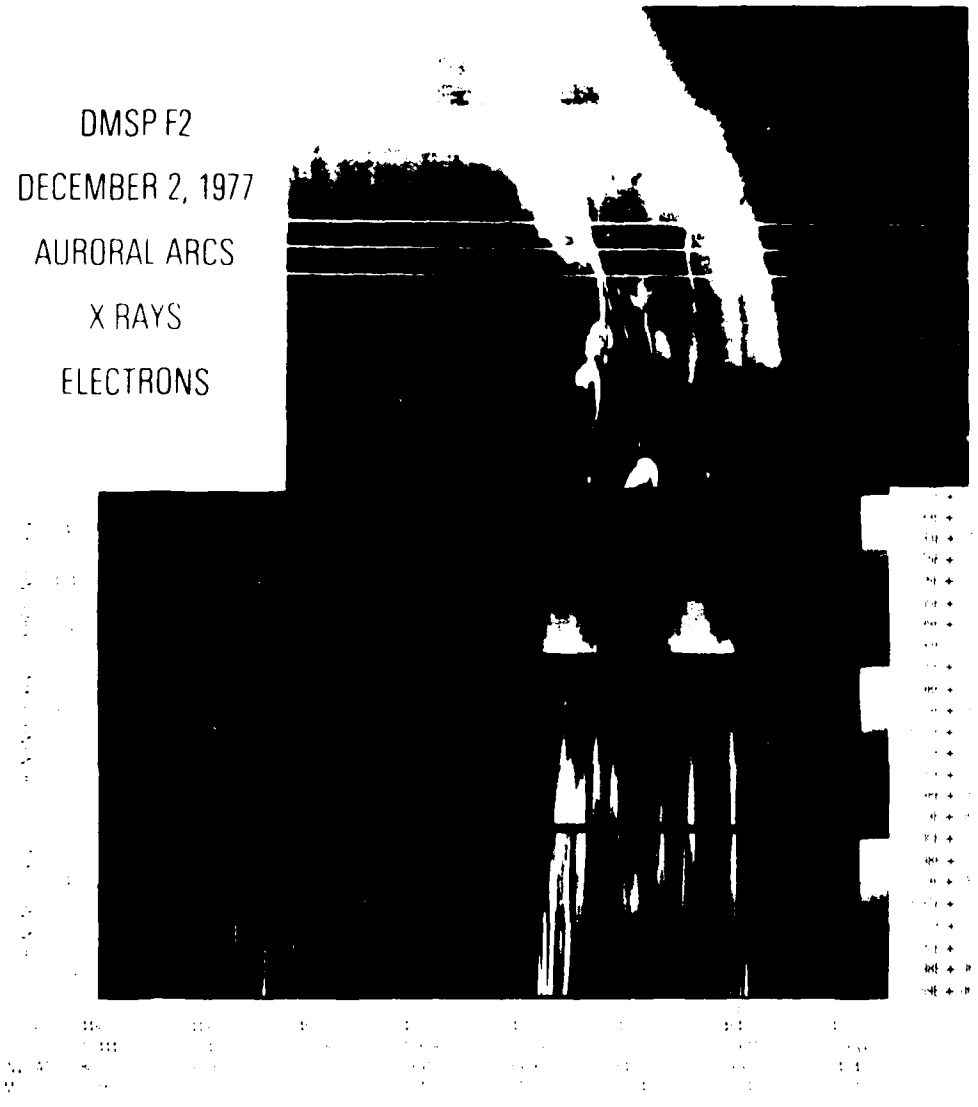

Fig. 3. Examples of Composite Auroral Photographs (top panels) and Spectrograms of Precipitating Electron Fluxes (bottom two panels) and Bremsstrahlung X-rays from the Atmosphere (middle panel). The auroral forms, X-rays and > 1 keV electron fluxes start at 45200 sec UT near Λ = 59.9°.

that in the inverted V, then no separate feature was distinguishable in the DMSP pictures. Also, the inverted V structure often appears as two half Vs with maximum energy flux at the juncture between the halves and strong flux enhancements over a wide range of energies at the same point. In many such cases the brightest part of the auroral form corresponded best to the position of the juncture.

This short survey implies that field alignment of electron fluxes over a wide range of energies may be a fairly common feature of the edges of the local evening and premidnight inverted V structures (see also Wahlen and Daly, 1979; Craven and Frank, 1975). We have not yet performed a statistical study to determine a probability of occurrence for the phenomenon.

Since all the above and previous observations have occurred at relatively low altitudes (< 1000 km), we used the S3-3 data set to see if this phenomenon was observed at higher altitudes. We have completed a preliminary search of the local evening data starting with low to intermediate altitudes (250-6000 km). The search turned up several candidates, most of which were at low altitudes (< 3000 km). Although we have examined large amounts of data in the 6000-8200 km altitude region, we have not found cases of strong field alignment in the electron fluxes over wide ranges of energies. In fact, it is relatively rare to find field aligned electrons at the higher altitudes. A more exhaustive study of the complete S3-3 local evening data base is in progress and may surface a few examples, but it appears that the phenomenon is a relatively low altitude one in this region.

Figure 4 is an example of an S3-3 spectrogram which shows the electron field alignment over a wide range of energies near 2110 UT at ~ 2400 km on April 3, 1978. The right panel shows a plot of the electron angular

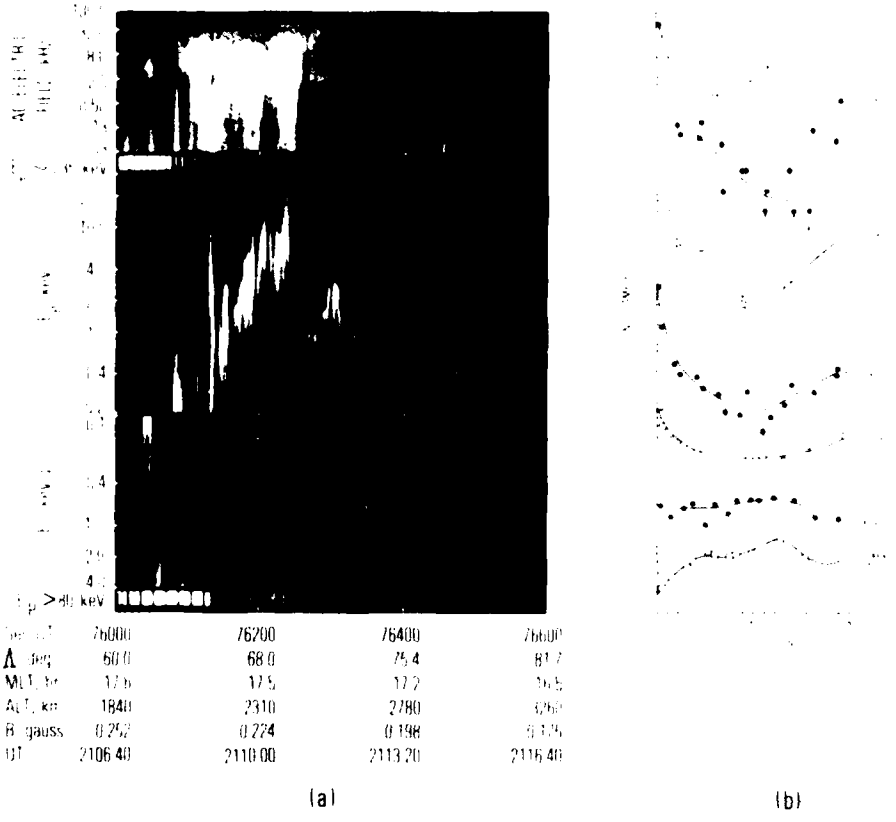

Figure 4

Fig. 4. (a) Spectrogram of S3-3 Satellite Data on April 3, 1977 near 2300 km.

(b) Pitch Angle Distribution of Intense Field Aligned Fluxes at the Edge of the Inverted V in Panel (a).

distributions channel by channel. Note that the maximum energy at which the field alignment occurs is low compared to the lower altitude examples in Fig. 2. The majority of the electron energy flux in the inverted V is carried by the $\geq$ 2 keV electrons. The field aligned electrons at the edge do not contribute significant energy flux. One would not, in this case, expect an auroral emission to correspond to the edge feature unless the electrons gain much more energy between 2400 km and the top of the atmosphere.

High Altitude Inverted V Structures

The S3-3 data may not contain examples of strong field alignment of the electron fluxes very often, but it does contain evidence of strong accelerations. In this section we will examine in some detail the particle distributions in an inverted V structure. The analysis emphasizes the information about the particle accelerations which is contained in the particle distributions, such as the total potential drop and the distribution of the potential above and below the satellite altitude as the structure is traversed. The inverted V in question has been discussed as part of a more inclusive analysis using the ion composition data, AC and DC electric fields and currents by Mizera et al. (1980).

The signatures we examine are impressed on the particles by the acceleration. These signatures are the enhanced electron loss cones and upflowing ions resulting from a potential drop existing below the spacecraft and strong peaks in the precipitating electron spectra evidencing the potential drops above the satellite. As is obvious from the terminology, it is assumed that the main acceleration mechanism acting is a field aligned quasi-static electric field.

Figure 5 is a spectrogram showing an inverted V signature in the electrons from 0255 to 0258 UT on September 6, 1976. The S3-3 satellite was at ~ 8000 km altitude near 18 MLT in the auroral zone. The ions corresponding to the inverted V are seen as upflowing beams and the electron loss cones are enhanced at low energies. These features are both indicative of a potential drop below the spacecraft which accelerates ions upward and electrons downward. The electron fluxes have peaked spectra (ref. Figure 7) indicative of a potential drop of the same sense existing above the spacecraft.

These particle signatures can be used to estimate the total potential drop, the potential drop above and the potential drop below the satellite as a function of latitude. This was done for this event and is presented as Figure 6. The potential profile has the appearance of two abutting inverted V structures with peak potential drops of 16-18 kV near 0256:10 UT and 12-14 kV near 0257:05 UT. The ratio of the potential drop below the satellite to that above the satellite, V_B/V_A, was not constant in this structure, as is shown in Figure 9a. It is clear that prior to the first peak in the total potential and after the second, the potential drop was primarily below the spacecraft. At the times of the peaks the potential drop was either equal above and below the satellite or slightly greater above (a factor of 2 or less).

In Figure 7 we show sample electron distribution functions and electron spectra taken at specific pitch angles. Figure 7a shows the plasmasheet electron distribution function measured just outside the inverted V structure. Figures 7b to 7d show the distribution functions measured just inside the inverted V, during the traversal of an electric field structure (see also Fig. 1 of Mizera et al., 1980) and just after traversing the electric field structure, respectively.

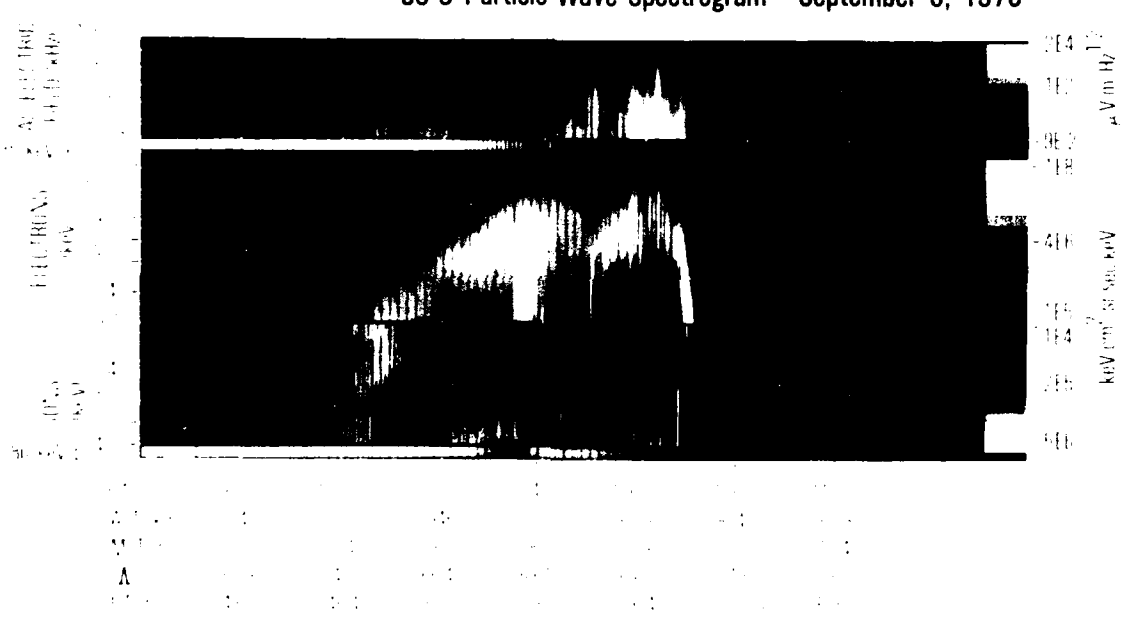

Fig. 5. Spectrogram of S3-3 Data Taken on September 6, 1976. An inverted V structure was encountered between 10500 and 10700 sec UT.

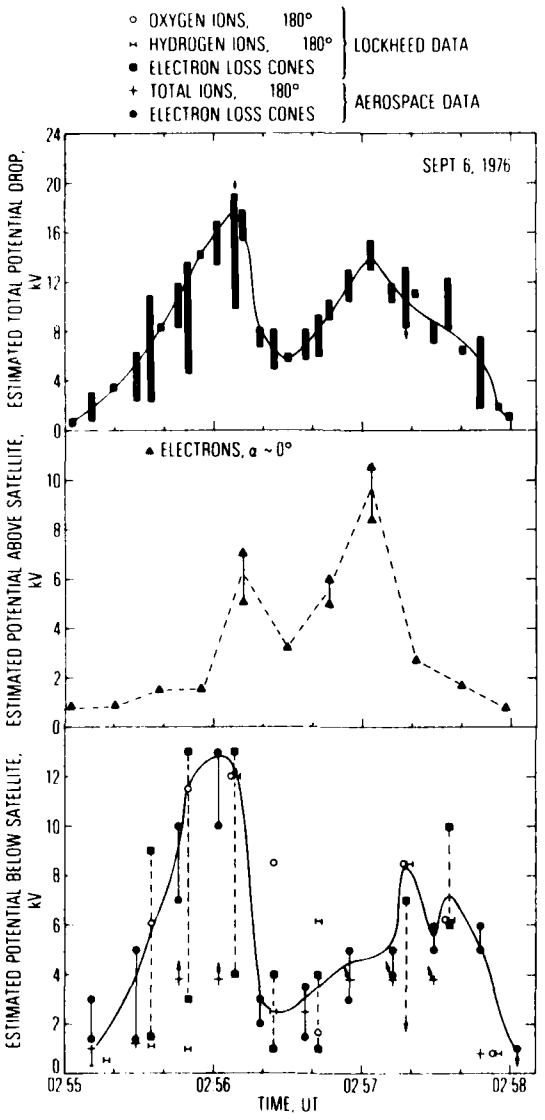

Fig. 6. Potential Drops Along the Magnetic Field Lines as Estimated from the Particle Data. The total potential drop (top panel), potential drop above the satellite (middle panel), and potential drop below the satellite (bottom panel) are estimated for the inverted V structure in Figure 5 (after Mizera et al., 1980).

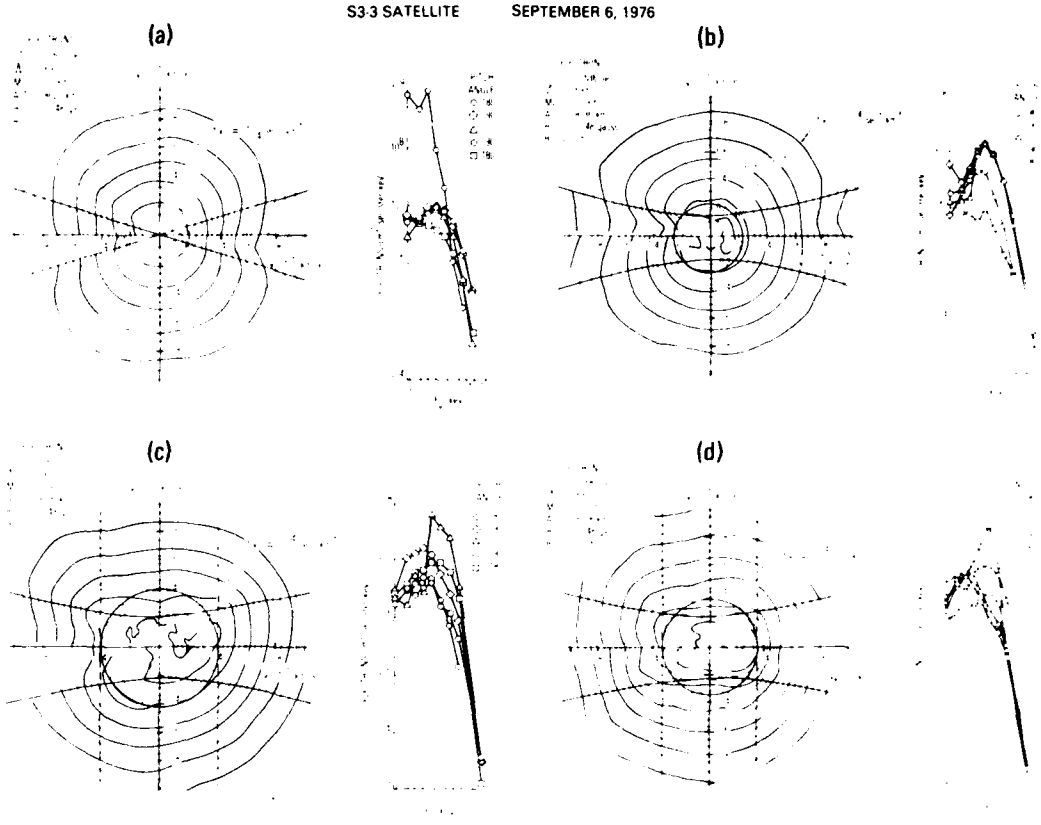

Fig. 7. (a) Ratio of Potential Drop Below to the Potential Drop Above the Satellite in the Inverted V Structure.

(b) Nomogram Relating the Ratio of the "Trapping" Region Boundary along $Vi_{\parallel}$ and $Vi_{\parallel}$ in Velocity Space to the Altitude at Which the Electron Acceleration Occurred for Observations at Three Different Satellite Altitudes. For details, see text.

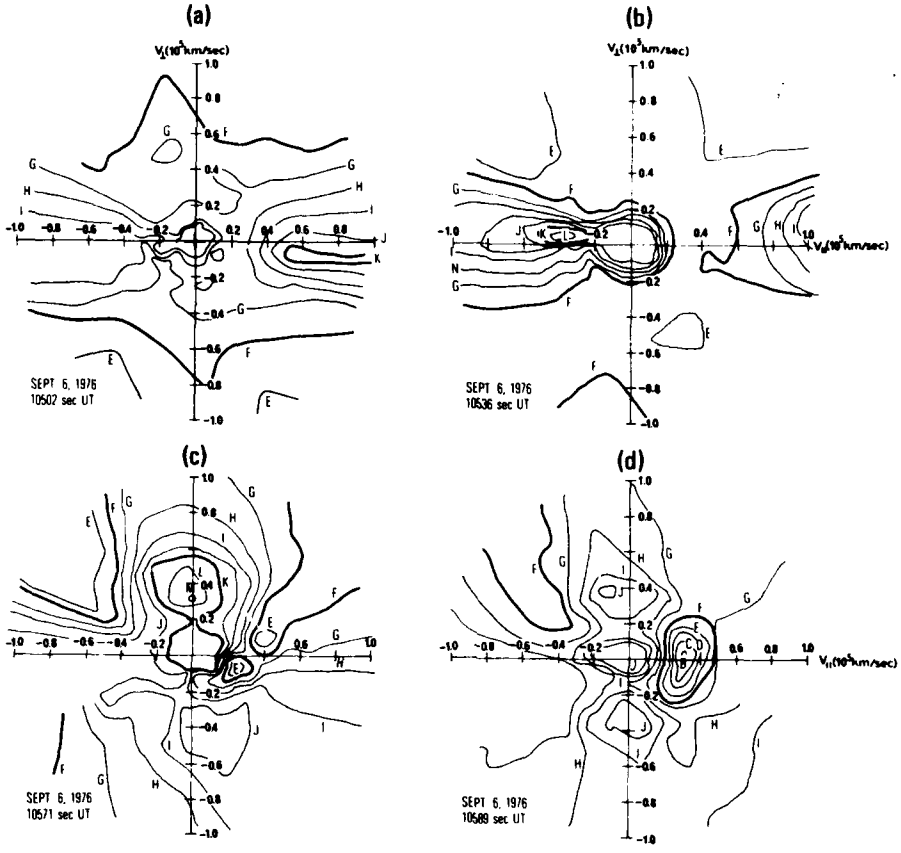

Fig. 8. Electron Isodistribution Function Contours in Velocity Space and Electron Energy Spectra at Specific Pitch Angles. Data taken in subauroral plasma sheet region (a), near low altitude edge of inverted V (b), at the time of electrostatic "shock" structure (c), and just after leaving electrostatic structure (d). For details, see text.

The straight lines which intersect at the origin in Figure 7a are the boundaries in velocity space corresponding to the 100 km atmospheric loss cone. We have assumed adiabatic motion of the electrons and that no potential drop existed below the satellite.

It has been shown (Whipple, 1977; Chiu and Schulz, 1978; Croley et al., 1978) that if the potential drop along a magnetic field line is the result of an electric field of suitable form, and one requires conservation of energy and the first adiabatic invariant, application of Lionville's theorem leads to equations representing particle boundaries in velocity space. The boundary for electrons which come from an arbitrary point below the spacecraft is a hyperbola in velocity space. The region of velocity space to which magnetospheric electrons (i.e., electrons which originate above the satellite) have no adiabatic access is bounded by an ellipse. The shape of the ellipse is determined by the distance to the upper bound of the potential drop. If the majority of that potential drop occurs very far above the satellite, the ellipse degenerates to a circle. If the majority of the potential drop above the satellite is local, the ellipse has a very high eccentricity. The region bounded between the ellipse and the hyperbola represents electrons trapped between their magnetic mirror points below the satellite and the potential drop which extends above the satellite (see Croley et al. (1978)). This can be represented by comparing the $V_{\parallel}$ and $V_{\perp}$ intercepts ($Vi_{\perp}$ and $Vi_{\parallel}$) of the ellipse and constructing a ratio $Vi_{\perp}/Vi_{\parallel}$ as a function of the altitude region where the majority of the potential drop would occur. Such a set of curves (one for each satellite altitude) would look like Figure 9b. Note that these curves are very insensitive to ratios that are either very large or very close to unity. In the intermediate range, the ratio $Vi_{\perp}/Vi_{\parallel}$ is a sensitive diagnostic of the extent of the potential drop. (For example, the ratio region

between ~ 1.3 and 2.0.).

In Figures 7b, 7c and 7d we have drawn on the distribution functions the ellipses and hyperbolas corresponding to potential drops of approximately 1.4 kV, 4 kV and 3 kV above the satellite and about 6 kV, 10 to 12 kV, and 4 to 8 kV below, respectively, for these data. The ellipses are represented by circles under the assumption that the majority of the potential drop above the spacecraft occurred far above the satellite. As can be seen, the circle is a pretty good match in Figure 7b but not so in Figures 7c and 7d. The distribution function plots in Figures 7c and 7d are clearly not well represented by a circular trapping boundary, but the most appropriate eccentricity is not clear. The hyperbolic loss cone boundaries represent the data well at high energies, but it is unclear whether they are appropriate for the low energy particles. The following analysis technique has been applied to better define these population boundaries.

The electron distribution function in Figure 7a can be taken as representative of the unaccelerated plasma sheet electrons. If a suitable functional form is fit to the velocity dependence of this plasma sheet distribution, outside the loss cone, one probably has a good representation of the unaccelerated source distribution for the auroral electrons. Subtracting this unaccelerated distribution from the measured distributions produces a display which indicates how particles have been redistributed in velocity space by the auroral potential drop. To obtain reasonable difference plots, the high energy tail of the source distribution is normalized to that of the measured distributions. Since the highest energies (10-30 keV) should be relatively unaffected by the potential drop above the spacecraft ($\lesssim$ 7 keV, see Fig. 6 of Mizera et al., 1980), the normalization should be valid and only the shape of the source distribution becomes important.

In Figure 8a the difference plot obtained by subtracting the smoothed source distribution from the measured plasma sheet distribution, of Figure 7a, is shown. Since the source distribution is assumed to be totally isotropic, the difference plot should show only the effect of a loss cone which exists in the real distribution. Contour F in the difference plot corresponds to zero difference. Contours G through M correspond to depletions and A through E represent enhancements of the measured distribution over the unaccelerated distribution. The contours are logarithmically spaced with five contour intervals corresponding to one order of magnitude. The straight lines which intersect at the origin, in Figure 7a, are the boundaries in velocity space corresponding to the 100 km atmospheric loss cone as discussed above. The measured loss cone is well represented in this plot, since most of the negative difference contours lie on or inside the region bounded by the straight lines.

This procedure was applied to each of the distributions in Figure 7 and the corresponding difference plots are shown in Figure 8. The same circles and hyperbolas used in Figure 7 are drawn on the difference plots 8b, 8c and 8d. Figure 8b shows a depletion in the loss cone and trapping region with the zero difference contour, F, corresponding very well to both the circle and hyperbola. This would indicate that for Figure 7b the distribution function is consistent with the potential drop above the satellite being predominantly far above the satellite.

Figures 8c and 8d show that a good match is attained between the hyperbola and the zero difference contour at the large parallel speeds ($> 0.4 \times 10^5$ km/sec and $> 0.35 \times 10^5$ km/sec, respectively). The zero contours extend parallel to the $V_\perp$ axes for these cases. The other contours such as H and I have elliptical shapes and we might estimate the contours cross the $V_\perp$ axis

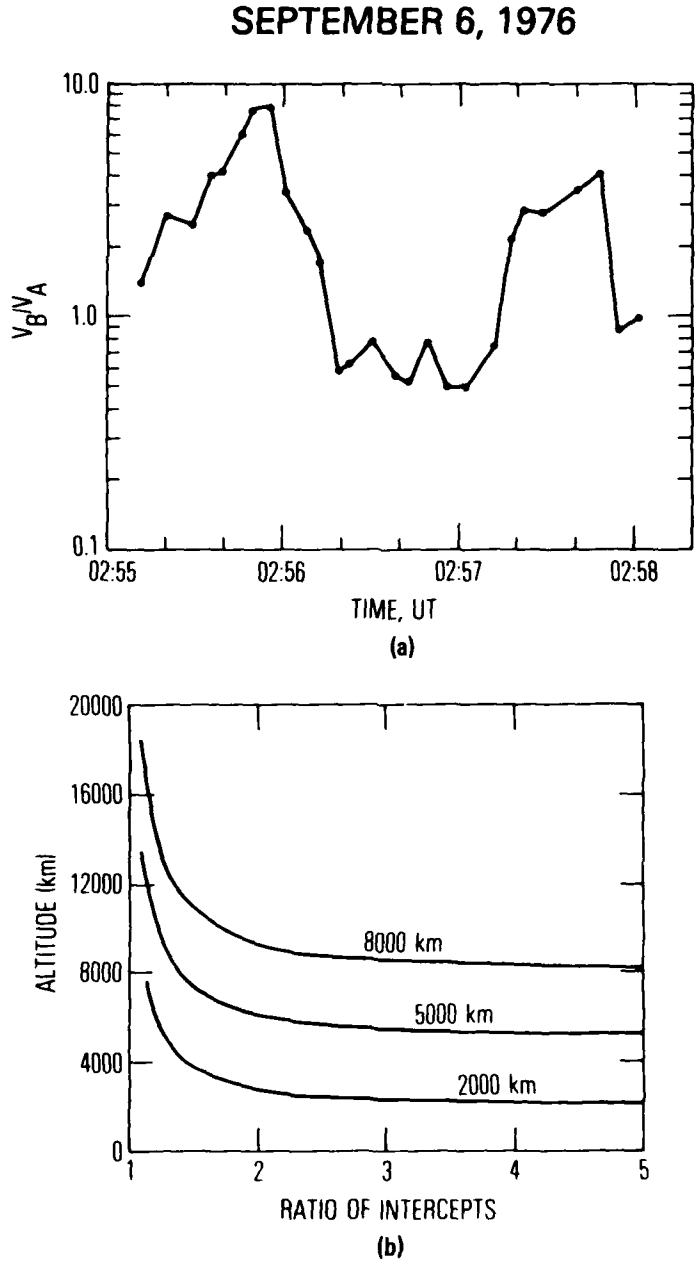

Fig. 9. Difference Plots Showing the Regions of Atmospheric Loss Cone and Trapping for the Distribution Functions of Figure 7. For discussion of boundary curves and differencing procedure, see text.

near 7 x 10^4 to 8 x 10^4 km/sec in Figure 8c and 4.5 x 10^4 to 5.5 x 10^4 km/sec in Figure 8d. The dashed lines show our estimate of the $V_{\parallel}$ intersection for a "best" ellipse based on the peak of the precipitating electron spectra. These correspond to ~ 3.6 x 10^4 km/sec for Figure 8c and ~ 3.0 x 10^4 km/sec for Figure 8d. The resulting ratios $Vi_{\perp}/Vi_{\parallel}$ are ~ 1.9 to 2.2 and ~ 1.5 to 1.8 for Figures 8c and 8d respectively. Comparing with Figure 9b for a satellite altitude of ~ 8000 km we see that the majority of the potential drop above the spacecraft is roughly within 1500-3000 km of the satellite for Figures 7c and 8c and ~ 3000-5000 km for Figures 7d and 8d.

Thus it appears that the technique of subtracting a source distribution from the measured one highlights the boundaries corresponding to the loss cone and trapping regions as defined above. This clear identification of particle boundaries yields information which allows the particle measurements to be used as diagnostics of the altitude distribution of the auroral potential drop.

Summary and Discussion

We have discussed two separate features of the auroral inverted V structure. The first part of the paper indicates that there is a lower altitude ($\lesssim$ 5000-6000 km) process acting which causes electrons to be precipitated and energized such that the angular distributions are highly field aligned over a wide range of energies. This process appears to be associated with the edges of the local evening inverted V structures. We cannot definitely conclude that the process occurs only in the presence of an inverted V structure. This must await a more systematic study of existing and new data.

These "edge" features appear to correlate with auroral brightening or arcs when their energy flux is high enough. Why they are seen preferentially in the low altitude data and what mechanism causes them is at this point unknown. It has been argued that they cannot result from quasistatic field aligned electric field acceleration but may be a result of acceleration by broadband electrostatic waves (Wahlen and Daly, 1979). Such a mechanism does not agree with the observations in detail, so at this point we can only emphasize that no complete quantitative description of this feature exists.

The second part of this report shows the kinds of information one can obtain using the particle distribution functions from the S3-3 observations. First, the case study presented showed that the total potential drop and the relative magnitude of the potential drops above and below an observation point can be determined. This determination was based on the assumption that the particle motions were adiabatic in a field aligned quasistatic electric field. A previous report (Mizera et al., 1980) showed that the ion beam energies and electron loss cone enhancements were consistent with those assumptions for the potential drop below the satellite.

The same assumptions were used in analyzing the particle distribution function features to determine the potential drop above the satellite and to make estimates of the altitude distribution of the potential drop.

In order to interpret the distribution function plots that were obtained during the occurrence of a large electrostatic structure (Mizera et al., 1980; Mozer et al., 1977; Torbert and Mozer, 1978), we had to generate a transformation procedure which produced a clearer display of the particle boundaries in velocity space. The boundaries themselves are based on the assumptions of adiabaticity, conservation of energy and electrostatic electric fields parallel to $\underline{B}$ (Chiu and Schulz, 1978; Croley et al., 1978; Whipple, 1977).

As a result, we found that the majority of the potential drop above the satellite at times occurred within a few thousand kilometers. If we combine this with the previous statistical results for field aligned ion beams which show that the potential drop corresponding to such ions normally operates above 4500 km (Ghielmetti et al., 1978; Gorney et al., 1980), we then conclude that the electrostatic potential drop corresponding to the electric field can assume various distributions in altitude, and at times can be confined to the low altitude (4500 - 100000 km) region.

References

Ackerson, K. L. and L. A. Frank, Correlated satellite measurements of low-energy electron precipitation and ground-based observations of a visible auroral arc, J. Geophys. Res., 77, 1128, 1972a.

Ackerson, K. L. and L. A. Frank, Correction, J. Geophys. Res., 77, 3002, 1972b.

Anger, C. D. and A. T. Y. Lui, A global view at the polar region on 18 December 1971, Planet. Space Sci., 21, 873, 1973.

Burch, J. L., S. A. Fields, W. B. Hansen, R. A. Heelis, R. A. Hoffman and R. W. Janetzke, Characteristics of auroral electron acceleration regions observed by Atmosphere Explorer C, J. Geophys. Res., 81, 2223, 1976.

Chiu, Y. T. and M. Schulz, Self consistent particle and parallel electrostatic field distributions in the magnetospheric-ionospheric auroral region, J. Geophys. Res., 83, 629, 1978.

Craven, J. D. and L. A. Frank, Observations of angular distributions of low energy electron intensities over the auroral zones with Ariel 4, Proc. R. Soc. Land. A., 343, 167, 1975.

Croley, D. R., Jr., P. F. Mizera and J. F. Fennell, Signature of a parallel electric field in ion and electron distributions in velocity space, J. Geophys. Res., 83, 2701, 1978.

Fennell, J. F., P. F. Mizera and D. R. Croley, Jr., Observations of ion and electron distributions during the July 29 and July 30, 1977 storm period, Proc. Magnetospheric Boundary Layers Conf., ESA SP-148, Alpbach, Austria, 1979.

Eather, R. H., DMSP calibration, J. Geophys. Res., 84, 4134, 1979.

Evans, D. S., Precipitating electron fluxes formed by a magnetic field aligned

potential difference, J. Geophys. Res., 79, 2853, 1974.

Frank, L. A. and K. L. Ackerson, Local-time survey of plasma at low altitudes over the auroral zones, J. Geophys. Res., 77, 4116, 1972.

Ghielmetti, A. G., R. G. Johnson, R. D. Sharp and E. G. Shelley, The latitudinal, diurnal and altitudinal distributions of upward flowing energetic ions of ionospheric origin, Geophys. Res. Lett., 5, 59, 1978.

Gorney, D. A., A. Clark, D. Croley, J. Fennell, J. Luhmann and P. Mizera, Auroral ion beam distributions below ~ 8000 km, J. Geophys. Res., 85, 83, 1980.

Hoffman, R. A. and J. L. Burch, Electron precipitation patterns and substorm morphology, J. Geophys. Res., 78, 2867, 1973.

Meng, C. I., Simultaneous observations of low energy electron precipitation and optical auroral arcs in the evening sector by the DMSP 32 satellite, J. Geophys. Res., 81, 2772, 1976.

Meng, C. I., Diurnal variation of the auroral oval size, J. Geophys. Res., 84, 5319, 1979.

Mizera, P. F., D. R. Croley, Jr., F. A. Morse and A. L. Vampola, Electron fluxes and correlations with quiet time auroral arcs, J. Geophys. Res., 80, 2129, 1975.

Mizera, P. F., D. R. Croley, Jr. and J. F. Fennell, Electron pitch-angle distributions in an inverted V structure, Geophys. Res. Lett., 3, 149, 1976.

Mizera, P. F. and J. F. Fennell, Signatures of electric fields from high and low altitude particle distributions, Geophys. Res. Lett., 4, 311, 1977.

Mizera, P. F., J. F. Fennell, D. R. Croley, Jr., A. L. Vampola, F. S. Mozer, R. B. Torbert, M. Temerin, R. Lysak, M. K. Hudson, C. A. Cattell, R. G. Johnson, R. D. Sharp, A. Ghielmetti and P. M. Kintner, The aurora inferred from S3-3 particles and fields, to be published, J. Geophys. Res., 85, 1980.

Mozer, F. S., C. W. Carlson, M. K. Hudson, R. B. Torbert, B. Parady, J. Yatteau and M. C. Kelley, Observations of paired electrostatic shocks in the polar magnetosphere, Phys. Rev. Lett., 38, 292, 1977.

Rogers, E. H., D. F. Nelson and R. C. Savage, Auroral photography from a satellite, Science, 183, 951, 1974.

Sharp, R. D., R. G. Johnson and E. G. Shelley, Energetic particle measurements from within ionospheric structures responsible for auroral precipitation processes, J. Geophys. Res., 84, 480, 1979.

Shelley, E. G., R. D. Sharp and R. G. Johnson, Satellite observations of an ionospheric acceleration mechanism, Geophys. Res. Lett., 3, 654, 1976.

Torbert, R. B. and F. S. Mozer, Electrostatic shocks as the source of discrete auroral arcs, Geophys. Res. Lett., 5, 1978.

Whalen, B. A. and P. W. Daly, Do field-aligned auroral particle distributions imply acceleration by quasi-static parallel electric fields?, J. Geophys. Res., 84, 4175, 1979.

Whipple, E. C., Jr., The signature of parallel fields in a collisionless plasma, J. Geophys. Res., 82, 1525, 1977.

Winningham, J. D., F. Yasuhara, S. -I. Akasofu and W. I. Heikkila, The latitudinal morphology of 10 eV to 10 keV electron fluxes during magnetically quiet and disturbed times in the 2100-0300 MLT sector, J. Geophys. Res., 80, 3148, 1975.

LABORATORY OPERATIONS

The Laboratory Operations of The Aerospace Corporation is conducting experimental and theoretical investigations necessary for the evaluation and application of scientific advances to new military space systems. Versatility and flexibility have been developed to a high degree by the laboratory personnel in dealing with the many problems encountered in the nation's rapidly developing space systems. Expertise in the latest scientific developments is vital to the accomplishment of tasks related to these problems. The laboratories that contribute to this research are:

Aerophysics Laboratory: Launch vehicle and reentry aerodynamics and heat transfer, propulsion chemistry and fluid mechanics, structural mechanics, flight dynamics; high-temperature thermomechanics, gas kinetics and radiation; research in environmental chemistry and contamination; cw and pulsed chemical laser development including chemical kinetics, spectroscopy, optical resonators and beam pointing, atmospheric propagation, laser effects and countermeasures.

Chemistry and Physics Laboratory: Atmospheric chemical reactions, atmospheric optics, light scattering, state-specific chemical reactions and radiation transport in rocket plumes, applied laser spectroscopy, laser chemistry, battery electrochemistry, space vacuum and radiation effects on materials, lubrication and surface phenomena, thermionic emission, photosensitive materials and detectors, atomic frequency standards, and bioenvironmental research and monitoring.

Electronics Research Laboratory: Microelectronics, GaAs low-noise and power devices, semiconductor lasers, electromagnetic and optical propagation phenomena, quantum electronics, laser communications, lidar, and electro-optics; communication sciences, applied electronics, semiconductor crystal and device physics, radiometric imaging; millimeter-wave and microwave technology.

Information Sciences Research Office: Program verification, program translation, performance-sensitive system design, distributed architectures for spaceborne computers, fault-tolerant computer systems, artificial intelligence, and microelectronics applications.

Materials Sciences Laboratory: Development of new materials: metal matrix composites, polymers, and new forms of carbon; component failure analysis and reliability; fracture mechanics and stress corrosion; evaluation of materials in space environment; materials performance in space transportation systems; analysis of systems vulnerability and survivability in enemy-induced environments.

Space Sciences Laboratory: Atmospheric and ionospheric physics, radiation from the atmosphere, density and composition of the upper atmosphere, aurorae and airglow; magnetospheric physics, cosmic rays, generation and propagation of plasma waves in the magnetosphere; solar physics, infrared astronomy; the effects of nuclear explosions, magnetic storms, and solar activity on the earth's atmosphere, ionosphere, and magnetosphere; the effects of optical, electromagnetic, and particulate radiations in space on space systems.

• • •